Synthesis, Crystal Structure, and Vibrational and Optical Spectroscopy of the First Quaternary Alkaline-Earth Rare Earth Thiophosphates $Ba_3Ln_2[P_4S_{16}]$ (Ln = Gd−Er)

Yvonne Klawitter,[†] Wolfgang Bensch,*[,†] and Claudia Wickleder[‡]

Institut für Anorganische Chemie, Universität Kiel, Olshausenstrasse 40, D-24098 Kiel, Germany, and Anorganische Chemie, Universität Siegen, D-57068 Siegen, Germany

Received August 18, 2005. Revised Manuscript Received October 28, 2005

The five quaternary compounds $Ba_3Gd_2[P_4S_{16}]$ (**1**), $Ba_3Tb_2[P_4S_{16}]$ (**2**), $Ba_3Dy_2[P_4S_{16}]$ (**3**), $Ba_3Ho_2[P_4S_{16}]$ (**4**), and $Ba_3Er_2[P_4S_{16}]$ (**5**) were synthesized at elevated temperatures in carbon-coated quartz tubes. The isostructural compounds crystallize in the orthorhombic space group *Pbcn* (No. 60), $Z = 4$, with $a = 19.127(3)$ Å, $b = 10.2795(5)$ Å, and $c = 12.648(2)$ Å for **1**; $a = 19.113(2)$ Å, $b = 10.261(2)$ Å, and $c = 12.616(2)$ Å for **2**; $a = 19.112(2)$ Å, $b = 10.2646(8)$ Å, and $c = 12.602(2)$ Å for **3**; $a = 19.088(3)$ Å, $b = 10.248(2)$ Å, and $c = 12.565(2)$ Å for **4**; and $a = 19.078(3)$ Å, $b = 10.241(2)$ Å, and $c = 12.568(2)$ Å for **5**.The structures are composed of one-dimensional infinite helical anionic $[Ln_2(PS_4)_4]_n^{6n-}$ chains and charge-compensating Ba^{2+} ions. The Ln atoms are surrounded by four $[PS_4]^{3-}$ tetrahedra, leading to a strong distorted LnS_8 rectangular antiprism. Three of the anions act as tetradentate ligands, and one is bidentate. Three Ln^{3+} centers are joined via one tetradentate $[PS_4]^{3-}$ ligand, and this connection mode yields helical anionic chains running along [001]. The structure of the title compounds may be regarded as being a member of the $(A_4P_2Q_6)_l(A_3PQ_4)_m(Ln_4(P_2Q_6)_3)_n(LnPQ_4)_o$ ($l = 0$, $m = 2$, $n = 0$, $o = 2$) family by replacing two A^+ ions by one Ba^{2+} cation. Furthermore, the structure is closely related to the two thiophosphates $K_3Ce_2[P_3S_{12}]$ and $K_3La[P_2S_8]$. Despite several similarities, the title compounds exhibit a new and unique structure type within the rare earth thiophosphates. All compounds are characterized with MIR; $Ba_3Gd_2[P_4S_{16}]$ and $Ba_3Er_2[P_4S_{16}]$ are further characterized with Raman/far-IR spectroscopy. Furthermore, the band gaps of all compounds are determined by reflectance spectroscopy. A detailed investigation of the $^5I_8 \leftrightarrow 4f^{10}$ transitions for $Ba_3Ho_2[P_4S_{16}]$ has been performed by means of reflectance as well as low-temperature luminescence spectroscopy. $Ba_3Ho_2[P_4S_{16}]$ shows a remarkably strong emission. The significant differences in the intensities of excitation bands compared to those of reflectance bands are explained by cross relaxation mechanisms.

Introduction

The interesting structural as well as physical properties of the MPS_3 type compounds (M = transition metal) as potential cathode materials[1] or for NLO applications[2] stimulated the intensive investigation of ternary and quaternary transition metal thiophosphates. In contrast, the exploration of rare earth (RE) thiophosphates was less intensive, and the number of compounds is relatively limited. However, since the structural characterization of the first RE thiophosphate $Eu_2[P_2S_6]$[3] and the discovery of the interesting luminescent properties of the $Ln[PS_4]$ family,[4−13] a series of new quaternary RE thiophosphates and selenophosphates has been reported. These compounds are $TlEu[PS_4]$,[14] $KLa[P_2Se_6]$,[15] $K_4Eu[PSe_4]_2$,[16] $KRE[P_2Se_6]$ (RE = Y, La, Ce, Pr, Gd),[17] $Rb_9Ce[PSe_4]_4$,[18] $A_3RE[P_2Se_8]$, $A_2RE[P_2Se_7]$ (A = Rb, Cs; RE = Ce, Gd),[19] $K_3Ce[P_2S_8]$,[20] $K_9Ce[P_4S_{16}]$,[21] $LiEu[PSe_4]$, $KEu[PSe_4]$,[22] $K_2La[P_2Q_7]$, $K_3La[PQ_4]_2$, $K_6La[PQ_4]_3$, $K_{9-x}La_{1+x/3}$-

* To whom correspondence should be addressed. E-mail: wbensch@ac.uni-kiel.de.
[†] Universität Kiel.
[‡] Universität Siegen.

(1) Le Mehaute, A.; Ouvrard, G.; Brec, R.; Rouxel, J. *Mater. Res. Bull.* **1977**, *12*, 1191.
(2) Langadic, I.; Lacroix, P. G.; Clément, R. *Chem. Mater.* **1997**, *9*, 2004.
(3) Brockner, W.; Becker, R. *Z. Naturforsch.* **1987**, *42A*, 511.
(4) Yampolàkaya, V. V.; Serebrennikov, V. V. *Russ. J. Inorg. Chem.* **1972**, *17*, 1771.
(5) Wibbelmann, C.; Brockner, W.; Eisenmann, B.; Schäfer, H. *Z. Naturforsch.* **1984**, *39*, 190.
(6) Palkina, K. K.; Maksimova, S. I.; Chibiskova, N. T.; Kuvshinova, T. B.; Volodina, A. N. *Inorg. Mater.* **1984**, *20*, 1557.
(7) Volodina, A. N.; Koubchinova, T. B.; Maximova, S. I.; Mouraviev, E. N.; Niazov, C. A.; Tchibiskova, N. I. *Zh. Neorg. Khim.* **1987**, *32*, 2899.
(8) Le Rolland, B.; Molinié, P.; Colombet, P. *C. R. Acad. Sci., Ser. II* **1990**, *310*, 1201.
(9) Le Rolland, B.; McMillan, P.; Molinié, P.; Colombet, P.. *Eur. J. Solid State Inorg. Chem.* **1990**, *27*, 715.
(10) Palkina, K. K.; Kuvshinova, T. B.; Maksimova, S. I.; Chibiskova, N. T.; Tirpolskaya, T. A. *Inorg. Mater.* **1989**, *25*, 1555.
(11) Huang, Z. L.; Cajipe, V.; Molinie, P. *J. Rare Earth* **1999**, *17*, 6.
(12) Huang, Z. L.; Cajipe, V.; Molinie, P. *J. Rare Earth* **1998**, *16*, 167.
(13) Huang, Z. L.; Cajipe, V.; Le Rolland, B.; Colombet, P.; Schnipper, W. J.; Blasse, G. *Eur. J. Solid State Inorg. Chem.* **1992**, *29*, 1133.
(14) Carillo-Cabrera, W.; Peters, K.; von Schnering, H. G. *Z. Anorg. Allg. Chem.* **1995**, *621*, 557.
(15) Chen, J. H.; Dorhout, P. K. *Inorg. Chem.* **1995**, *34*, 5705.
(16) Chondroudis, K.; McCarthy, T. J.; Kanatzidis, M. G. *Inorg. Chem.* **1996**, *35*, 840.
(17) Chen, J. H.; Dorhout, P. K.; Ostenson, J. E. *Inorg. Chem.* **1996**, *35*, 5627.
(18) Chondroudis, K.; Kanatzidis, M. G. *Inorg. Chem. Commun.* **1998**, *1*, 55.
(19) Chondroudis, K.; Kanatzidis, M. G. *Inorg. Chem.* **1998**, *37*, 3792.
(20) Gauthier, G.; Jobic, S.; Brec, R.; Rouxel, J. *Inorg. Chem.* **1998**, *37*, 2332.

10.1021/cm051860n CCC: $33.50
Published on Web 11/30/2005

$[PQ_4]_4$ ($x = 0.5$), KEu$[PQ_4]$ (Q = S, Se), KLa$[P_2S_6]$, K_4Eu$[P_2S_6]$,[23,24] NaYb$[P_2S_6]$, NaSm$[P_2S_6]$, KSm$[P_2S_7]$,[25] NaCe$[P_2Se_6]$, $Cu_{0.4}Ce_{1.2}[P_2Se_6]$, $Ce_4[P_2Se_6]_3$, AgCe$[P_2Se_6]$,[26] K_2Nd$[P_2S_7]$,[27] $K_3Ce_2[P_3S_{12}]$,[28] $Rb_3M_3[PS_4]_4$ (M = Pr, Er),[29] $K_6Yb_3[PS_4]_5$,[30] LiEu$[PS_4]$,[31] $Cs_3Pr_5[PS_4]_6$,[32] $Cs_4Pr_2[PS_4]_2[P_2S_6]$,[33] and $Li_9Gd_2[PS_4]_5$,[34] with structures ranging from separated ions to one-dimensional chains over two-dimensional layers to three-dimensional networks.

Most of these compounds contain alkali metals, and they were often prepared applying the so-called molten flux technique. Interestingly, until now no RE thiophosphates containing alkaline-earth metal cations have been reported. Another interesting point is that there are only a few systematic investigations about the influence of the radius of RE ions on the crystal structure using identical reaction conditions. The overwhelming number of compounds with RE thiophosphates was obtained with only two different RE ions.

In the present paper, we report the syntheses and crystal structure of the first quaternary alkaline-earth RE thiophosphates $Ba_3Ln_2[P_4S_{16}]$ (Ln = Gd−Er). With the intention of synthesizing new compounds with interesting luminescence behavior that are probably more stable than the extremely air-sensitive compounds of the Ln$[PS_4]$ family, we found that $Ba_3Ho_2[P_4S_{16}]$ shows noteworthy luminescence properties.

Experimental Section

Synthesis. All starting materials (BaS, 99.99% purity, Alfa; P_2S_5, 99.99%, Alfa; S, 99.99%, Heraeus; $BaCl_2$, 99.99%, Fluka; Gd, Dy, Tb, and Ho, 99.99%, <200 mesh, REacton; Er, 99.99%, <40 mesh, Chempur) were thoroughly mixed in a N_2-filled glovebox, and were transferred into a carbon-coated quartz ampule. After evacuation to 10^{-3} mbar, the ampules were flame-sealed and placed in a computer-controlled furnace. An EDX analysis of the single crystals indicated the presence of all four elements (Ba, Ln, P, S) in each case, in an approximate atomic ratio of 3:2:4:16. All compounds are moisture sensitive. For the different compounds, it was necessary to find the optimal synthesis conditions, and consequently the actual temperature profiles and annealing times are different for different samples.

Preparation of $Ba_3Gd_2[P_4S_{16}]$, $Ba_3Dy_2[P_4S_{16}]$, and $Ba_3Er_2[P_4S_{16}]$. Crystals large enough for X-ray studies were obtained by reacting a mixture of BaS (0.48 mmol), Ln (0.48 mmol), P_2S_5 (0.48 mmol), S (0.96 mmol), and $BaCl_2$ (0.46 mmol) as flux in the molar ratio 1:1:1:2:1. The ampule was heated to 1273 K within 83 h. After 3 days, the product was cooled to 1073 K at a cooling rate of 6 K h^{-1}, and was subsequently cooled to 773 K at 9 K h^{-1}, and to 373 K at 24 K h^{-1}; the mixture was finally quenched by switching off the furnace. The product was washed with DMF and, carefully, with a water/acetone mixture (1:4 vol %) to remove residual $BaCl_2$. The final product consists of yellow crystals (in the case of Dy and Gd) or pink crystals (Er).

Preparation of $Ba_3Tb_2[P_4S_{16}]$. Crystals suitable for X-ray studies were obtained by heating a mixture of BaS (0.4 mmol), Tb (0.4 mmol), P_2S_5 (0.4 mmol), and S (2.4 mmol) in the molar ratio 1:1:1:6. The ampule was heated to 1273 K within 83 h. After 3 days, the sample was cooled to 1073 K at a cooling rate of 6 K h^{-1}, and was subsequently cooled to 773 K at 9 K h^{-1}, and to 373 K at 24 K h^{-1}; the mixture was finally quenched at room temperature. After washing with DMF and acetone, we obtained yellow crystals.

Preparation of $Ba_3Ho_2[P_4S_{16}]$. The reaction of a mixture of BaS (0.48 mmol), Ho (0.48 mmol), P_2S_5 (0.48 mmol), and S (0.96 mmol) in the molar ratio 1:1:1:2 yields crystals suitable for single-crystal X-ray work. The mixture was heated to 1273 K within 150 h. This temperature was kept for 3 days before the product was cooled to 873 K at a cooling rate of 8 K h^{-1}. Afterward, the ampule was cooled to room temperature at 33 K h^{-1}. The product was washed with DMF and acetone, yielding yellow crystals.

Crystallography. Single-crystal X-ray work was performed using a Philips PW 1100 or a STOE Imaging Plate Diffraction System (IPDS) (Mo Kα radiation; $\lambda = 0.71073$ Å). The raw intensities were treated in the usual way, applying a Lorentz, polarization, and face-indexed absorption correction. Structure solution was performed with SHELXS-97.[35] Refinement was done against F^2 using SHELXL-97.[35] All atoms were refined with anisotropic displacement parameters. Technical details of the data acquisition as well as some refinement results are summarized in Table 1, and atomic coordinates and equivalent isotropic displacement parameters are given in Table 2 for $Ba_3Gd_2[P_4S_{16}]$.

The data in the Supporting Information have been sent to the Fachinformationszentrum Karlsruhe, Abt. PROKA, 76344 Eggenstein-Leopoldshafen, Germany, as CSD415877 (**1**), CSD415875 (**2**), CSD415878 (**3**), CSD415876 (**4**), and CSD415986 (**5**), and can be obtained by contacting the FIZ.

Physical Property Measurements. MIR spectra (4000−400 cm^{-1}, 2 cm^{-1} resolution) were collected on a Genesis FT-spectrometer (ATI Mattson). UV−vis spectroscopic investigations were conducted at room temperature using a UV−vis−NIR two-channel Cary 5 spectrometer from Varian Techtron. The optical properties of all five compounds were investigated by studying the UV−vis reflectance spectrum. Samples were prepared by grinding them to a fine powder. The reflectance data were converted to absorption data through the Kubelka−Munk relation for diffuse reflectance data. $BaSO_4$ powder was used as a reflectance standard.

Semiquantitative microprobe analysis was performed with a Philips ESEM XL 30 scanning electron microscope equipped with an EDAX analyzer.

Emission and excitation spectra were recorded at room temperature as well as at 77 K using a spectrofluorometer (Fluorolog 3, Jobin-Yvon) equipped with two 0.22 m double monochromators (SPEX, 1680) and a 150 W xenon lamp. The emission spectra were corrected for photomultiplier sensitivity, the excitation spectra for lamp intensity, and both for the transmission of the monochromators.

(21) Gauthier, G.; Jobic, S.; Danaire, V.; Brec, R.; Evain, M. *Acta Crystallogr., Sect. C* **2000**, *56*, e117.
(22) Aitken, J.; Chondroudis, K.; Young, V. G., Jr.; Kanatzidis, M. G. *Inorg. Chem.* **2000**, *39*, 1525.
(23) Evenson, C. R., IV; Dorhout, P. K. *Inorg. Chem.* **2001**, *40*, 2875.
(24) Evenson, C. R., IV; Dorhout, P. K. *Inorg. Chem.* **2001**, *40*, 2884.
(25) Goh, E.-Y.; Kim, E.-J.; Kim, S.-J. *J. Solid State Chem.* **2001**, *160*, 195.
(26) Aitken, J.; Evain, M.; Iordanidis, L.; Kanatzidis, M. G. *Inorg. Chem.* **2002**, *41*, 180.
(27) Schleid, T.; Hartenbach, I.; Komm, T. *Z. Anorg. Allg. Chem.* **2002**, *628*, 7.
(28) Gauthier, G.; Evain, M.; Jobic, S.; Brec, R. *Solid State Sci.* **2002**, *4*, 1361.
(29) Komm, T.; Schleid, T. *J. Solid State Chem.* **2005**, *178*, 454.
(30) Aitken, J. A.; Kanatzidis, M. G. *J. Am. Chem. Soc.* **2004**, *126*, 11780.
(31) Jörgens, S.; Alili, L.; Mewis, A. *Z. Naturforsch.* **2005**, *60b*, 705.
(32) Komm, T.; Schleid, T. *Z. Anorg. Allg. Chem.* **2004**, *630*, 712.
(33) Komm, T.; Schleid, T. *Z. Kristallogr. Suppl.* **2003**, *20*, 152.
(34) Komm, T.; Schleid, T. *Z. Kristallogr. Suppl.* **2005**, *22*, 162.
(35) Sheldrick, G. M. *SHELXS-97 and SHELXL-97, Programs for the Solution and Refinement of Crystal Structures*; Universität Göttingen: Göttingen, Germany, 1997.

Table 1. Technical Details of Data Acquisition and Some Refinement Results for $Ba_3Ln_2[P_4S_{16}]$ (measuring temperature: 293 K; space group: *Pbcn*; $Z = 4$)

	$Ba_3Gd_2[P_4S_{16}]$	$Ba_3Tb_2[P_4S_{16}]$	$Ba_3Dy_2[P_4S_{16}]$	$Ba_3Ho_2[P_4S_{16}]$	$Ba_3Er_2[P_4S_{16}]$
a (Å)	19.127(3)	19.113(2)	19.112(2)	19.088(3)	19.078(3)
b (Å)	10.2795(5)	10.261(2)	10.2646(8)	10.248(2)	10.241(2)
c (Å)	12.648(2)	12.616(2)	12.602(2)	12.565(2)	12.568(2)
V (Å^3)	2486.8(5)	2474.2(5)	2472.2(4)	2457.9(7)	2455.6(7)
d_{calcd} (g cm^{-3})	3.641	3.669	3.691	3.726	3.742
cryst color	colorless	pale yellow	pale yellow	yellow	pink
μ (mm^{-1})	11.53	11.95	12.28	12.71	13.11
F(000)	2448	2456	2464	2472	2480
scan range	$3° \le 2\theta \le 60°$	$3° \le 2\theta \le 54°$	$3° \le 2\theta \le 54°$	$3° \le 2\theta \le 60°$	$5° \le 2\theta \le 56°$
index range	$-24 \le h \le 1$, $-13 \le k \le 1$, $-16 \le l \le 1$	$-24 \le h \le 1$, $-13 \le k \le 1$, $-16 \le l \le 1$	$-24 \le h \le 1$, $-13 \le k \le 6$, $-16 \le l \le 1$	$-26 \le h \le 1$, $-14 \le k \le 14$, $-17 \le l \le 1$	$-23 \le h \le 23$, $-13 \le k \le 13$, $-16 \le l \le 16$
no. of reflns collected	3392	3200	4851	7992	22508
no. of independent reflections	2692	2703	2699	3591	2845
R_{int}	0.022	0.0541	0.0289	0.0543	0.0557
min./max. transmittance	0.1914/0.2454	0.1716/0.2311	0.1968/0.3454	0.2631/0.3695	0.0425/0.3039
reflns with $F_o > 4\sigma(F_o)$	2272	1920	2328	2815	2687
no. of params	115	115	115	115	115
x[a]	0.1025	0.0915	0.0564	0.0333	0.0345
y[a]	45.64	63.89	6.57	5.52	12.7108
R_1 for $F_o > 4\sigma(F_o)$	0.0463	0.0474	0.0275	0.0294	0.0272
wR_2 for all reflections	0.1613	0.1621	0.0985	0.0729	0.0682
GOF	1.103	1.061	1.217	1.023	1.142
$\Delta\rho$ (e Å^{-3})	−3.20/3.41	−2.31/3.51	−1.87/2.10	−1.75/1.67	−1.7/1.01

[a] $w = 1/[\sigma^2(F_o^2) + (xP)^2 + yP]$; $P = (\max(F_o^2, 0) + 2F_c^2)/3$.

Table 2. Atomic Coordinates ($\times 10^4$) and Equivalent Isotropic Displacement Parameters U_{eq} (Å^2 $\times$ 10^3) for $Ba_3Gd_2[P_4S_{16}]$[a]

	x	y	z	U_{eq}
Gd	5737(1)	1286(1)	1129(1)	16(1)
Ba(1)	7279(1)	−2892(1)	−1111(1)	22(1)
Ba(2)	5000	−3804(1)	2500	24(1)
P(1)	3968(2)	−43(3)	1396(2)	17(1)
P(2)	6310(2)	−5597(3)	483(2)	18(1)
S(1)	6505(2)	−3815(3)	1054(2)	26(1)
S(2)	6464(2)	−5685(3)	−1126(2)	20(1)
S(3)	4833(2)	−1129(3)	1005(2)	20(1)
S(4)	6930(2)	−2950(3)	1141(2)	20(1)
S(5)	4302(1)	1812(3)	1674(2)	20(1)
S(6)	5320(2)	3835(3)	861(3)	23(1)
S(7)	6688(1)	−69(3)	−148(2)	22(1)
S(8)	6529(2)	−675(3)	2312(2)	25(1)

[a] Estimated standard deviations are given in parentheses. The U_{eq} is defined as one-third of the trace of the orthogonalized U_{ij} tensor.

Results and Discussion

Crystal Structure. In the structures of $Ba_3Ln_2[P_4S_{16}]$ (Ln = Gd, Tb, Dy, Ho, Er), one unique Ln atom, two crystallographically independent Ba cations, eight unique S atoms, and two independent P atoms are observed. With the exception of Ba(2), all atoms are on general positions. The Ln^{3+} ions are in a distorted rectangular antiprismatic coordination of eight S atoms (Figure 1). Two S atoms belong to a bidentate $[P(2)S_4]^{3-}$ unit, whereas the other S atoms are from three tetradentate $[P(1)S_4]^{3-}$ tetrahedra, each of them connecting two further Ln^{3+} ions (Figure 2, top). The LnS_8 antiprisms are joined by sharing edges with two neighboring LnS_8 polyhedra (Figure 2, bottom). The connection of three Ln^{3+} ions via one tetradentate $[PS_4]^{3-}$ tetrahedron leads to the formation of $[Ln_2(PS_4)_4]_n^{6n-}$ anionic chains running along [001] (Figure 3). These chains are separated by the two independent Ba atoms with Ba(1) in a 9-fold and Ba2 in an 8-fold coordination. The Ba(1) atoms separate the chains in the [100] direction, and the Ba(2) atoms are located between the chains along [010]. Note that along

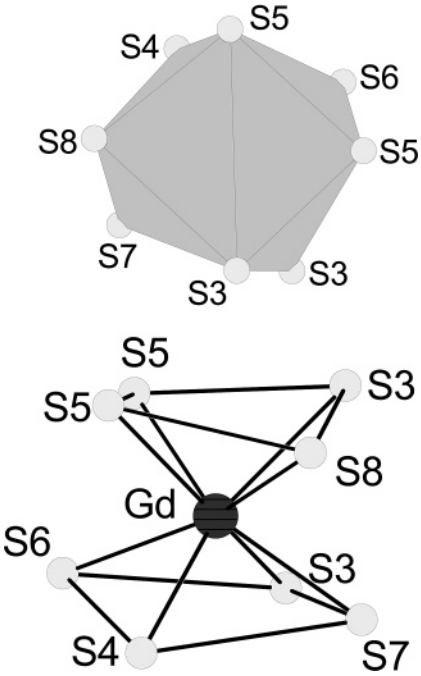

Figure 1. Distorted GdS_8 antiprism in $Ba_3Gd_2[P_4S_{16}]$.

the chain direction, distances between neighboring Ln atoms alternate in a long−short−long fashion. With the exception of Ho, the distances between Ln^{3+} centers show the expected behavior (Figure 4; Table 3). In accordance with the unusual behavior of Ho, the c axis significantly deviates from linearity (Figure 5, top) and slight deviations from the expected linear behavior are also observed for Dy (a axis) and for Tb (b axis) (Figure 5, top). The Ln−S distances ranging from 2.761(3) to 3.029(3) Å (Gd), 2.749(4) to 3.021(4) Å (Tb), 2.743(2) to 3.013(2) Å (Dy), 2.731(2) to 3.005(2) Å (Ho), and 2.724(2) to 3.001(2) Å (Er) (Table 3) follow the trend of the Ln^{3+} radii. The average Ln−S distances are 2.876 (calcd 2.893), 2.865 (calcd 2.880), 2.858 (calcd 2.867), 2.846

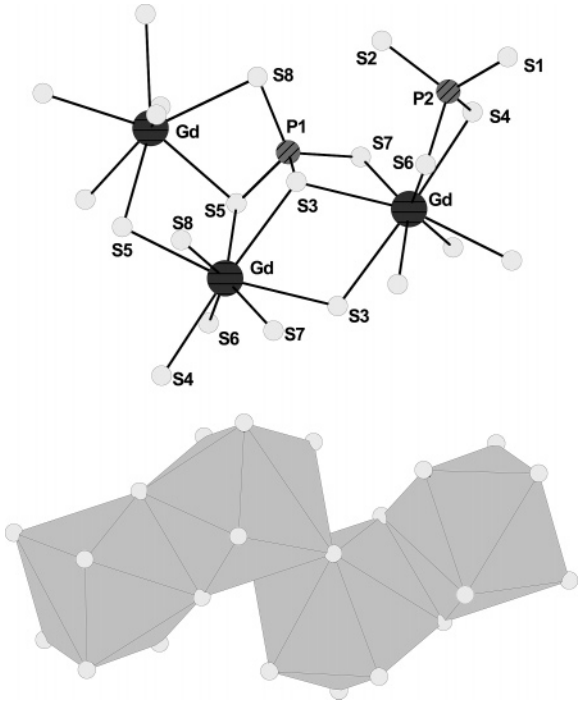

Figure 2. Interconnection of three GdS_8 polyhedra by the central $[P(1)S_4]^{3-}$ tetrahedron and the connectivity of the $[P(2)S_4]^{3-}$ tetrahedron (top). Polyhedral representation of the chain of interconnected LnS_8 polyhedra (bottom).

(calcd 2.855), and 2.841 Å (calcd 2.844). The distances monotonically decrease with the size of the Ln^{3+} ions (Figure 5, bottom), in good agreement with the sum of the ionic radii for Ln^{3+} and S^{2-}.[36]

In the following, the discussion of the structure refers to $Ba_3Gd_2[P_4S_{16}]$. The corresponding geometric parameters for all compounds are summarized in Table 3.

The LnS_8 antiprisms are strongly distorted, as evidenced by the torsion angles that deviate from the ideal value of 45° between the planes formed by S5−S5−S3−S8 and S6−S3−S7−S4 (compare Figure 1). Furthermore, the distortion is evidenced by the four different S−S distances in each plane, ranging from 3.271(5) to 3.669(5) Å for the plane S5−S5−S3−S8 and scattering between 2.231(5) and 3.660-(5) Å for S3−S6−S4−S7.

Table 3. Selected Geometric Parameters (Å, deg) for Compounds $Ba_3Ln_2[P_4S_{16}]$

	Gd	Tb	Dy	Ho	Er
Ln−S6	2.761(3)	2.749(4)	2.743(2)	2.731(2)	2.724(2)
Ln−S5	2.832(3)	2.822(4)	2.810(2)	2.790(2)	2.787(2)
Ln−S5	2.882(3)	2.871(3)	2.866(2)	2.860(2)	2.857(2)
Ln−S8	2.931(3)	2.917(4)	2.914(2)	2.904(2)	2.901(2)
Ln−S7	2.803(3)	2.786(4)	2.782(2)	2.770(2)	2.763(2)
Ln−S4	2.852(3)	2.845(4)	2.837(2)	2.824(2)	2.814(2)
Ln−S3	2.916(3)	2.907(4)	2.901(2)	2.885(2)	2.884(2)
Ln−S3	3.029(3)	3.021(4)	3.013(2)	3.005(2)	3.001(2)
Ln−Ln(min)	4.469(2)	4.457(2)	4.449(7)	4.434(1)	4.442(2)
Ln−Ln(max)	4.805(2)	4.795(2)	4.788(2)	4.775(1)	4.776(1)
⟨Ln−Ln⟩	4.637	4.625	4.618	4.605	4.609
S3−S8	3.396(5)	3.408(6)	3.413(3)	3.410(3)	3.408(3)
S5−S7	3.244(5)	3.249(6)	3.253(3)	3.249(3)	3.256(3)
S1−P2	2.004(4)	2.006(5)	2.006(2)	2.008(2)	2.008(3)
S4−P2	2.080(4)	2.073(5)	2.072(2)	2.070(2)	2.072(2)
S2−P2	2.058(4)	2.059(6)	2.062(2)	2.054(3)	2.059(3)
S6−P2	2.039(4)	2.045(5)	2.046(3)	2.041(3)	2.042(3)
S3−P1	2.057(4)	2.055(5)	2.059(3)	2.055(2)	2.053(2)
S7−P1	2.020(4)	2.027(5)	2.025(2)	2.019(3)	2.022(2)
S5−P1	2.041(4)	2.039(5)	2.045(2)	2.039(2)	2.039(2)
S8−P1	1.998(4)	2.006(5)	1.999(2)	1.997(3)	1.993(3)
S1−P2−S6	110.5(2)	110.3(2)	110.5(2)	110.6(1)	110.6(1)
S6−P2−S2	110.7(2)	110.6(2)	110.4(2)	110.6(1)	110.4(1)
S6−P2−S4	103.3(2)	103.5(2)	103.3(2)	103.(1)	102.9(1)
S1−P2−S2	111.7(2)	111.3(2)	111.2(2)	111.2(1)	111.3(1)
S1−P2−S4	113.9(2)	114.2(2)	114.5(2)	114.6(1)	114.6(1)
S2−P2−S4	106.4(2)	106.6(2)	106.6(2)	106.6(2)	106.7(1)
S7−P1−S5	106.0(2)	106.1(2)	106.1(2)	106.4(1)	106.6(1)
S7−P1−S3	110.0(2)	109.7(2)	109.7(2)	109.4(1)	109.1(1)
S8−P1−S5	108.2(2)	107.9(2)	107.6(2)	107.3(1)	107.2(1)
S8−P1−S3	113.7(2)	114.1(1)	114.5(2)	114.6(1)	114.8(1)
S5−P1−S3	107.3(2)	107.4(2)	107.3(2)	107.3(1)	107.1(1)
S8−P1−S7	111.3(2)	111.3(2)	111.2(2)	111.4(1)	111.7(1)
S3−Ln−S3	72.14(9)	72.03(12)	71.91(5)	71.68(4)	71.50(4)
S5−Ln−S5	72.82(9)	72.69(12)	72.40(6)	72.28(4)	71.97(4)

The GdS_8 polyhedra are bridged by two independent $[PS_4]^{3-}$ tetrahedra. The central $[P(1)S_4]^{3-}$ group acts as a tetradentate ligand, and $[P(2)S_4]^{3-}$ is bidentate with S(1) and S(2) remaining terminal (Figure 2, top). The $[P(1)S_4]^{3-}$ tetrahedron shares three edges with three GdS_8 polyhedra, whereas $[P(2)S_4]^{3-}$ has only one common edge with a GdS_8 polyhedron. The $[P(1)S_4]^{3-}$ unit is moderately distorted (S−P−S angles: 106.0(2)−113.7(2)°; Table 3). A slightly stronger distortion is observed for $[P(2)S_4]^{3-}$, with S−P−S angles from 103.3(2) to 113.9(2)°. The bond lengths in the two tetrahedra are comparable (Table 3), and the average

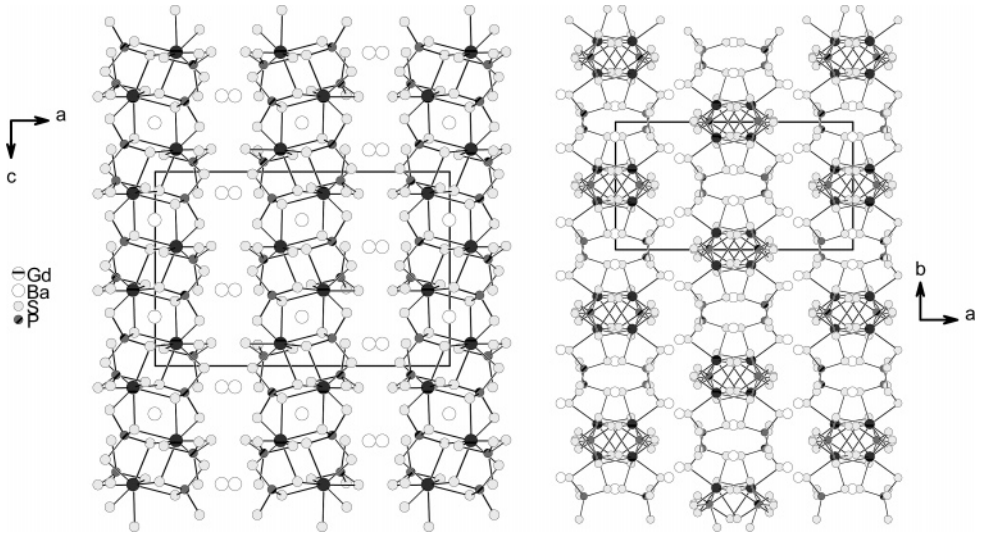

Figure 3. Two different views of the helical anionic chains in $Ba_3Gd_2[P_4S_{16}]$.

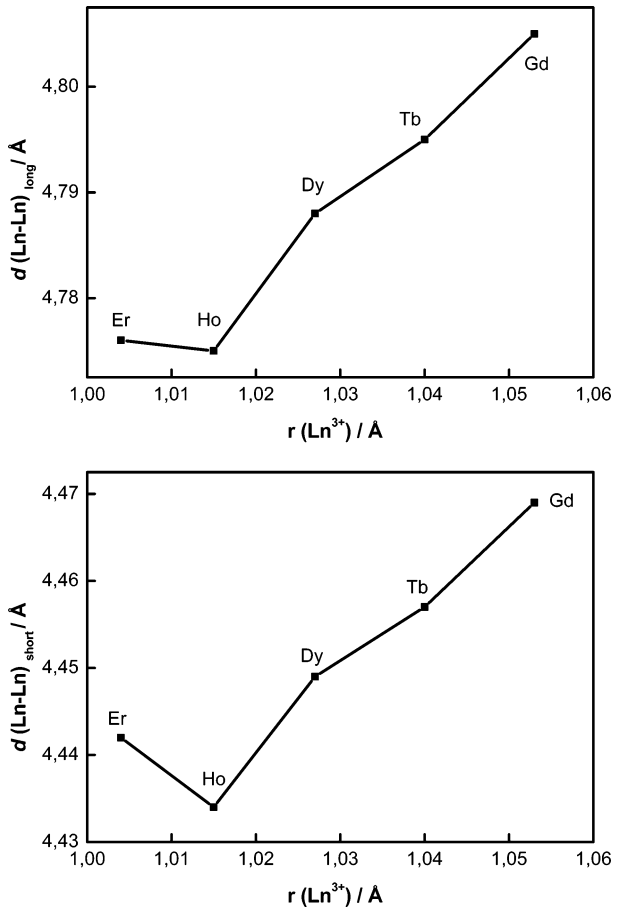

Figure 4. Evolution of the two different Ln−Ln distances across the series $Ba_3Ln_2[P_4S_{16}]$ (Ln = Er, Ho, Dy, Tb, Gd). Short Ln−Ln separations (top), long Ln−Ln separations (bottom).

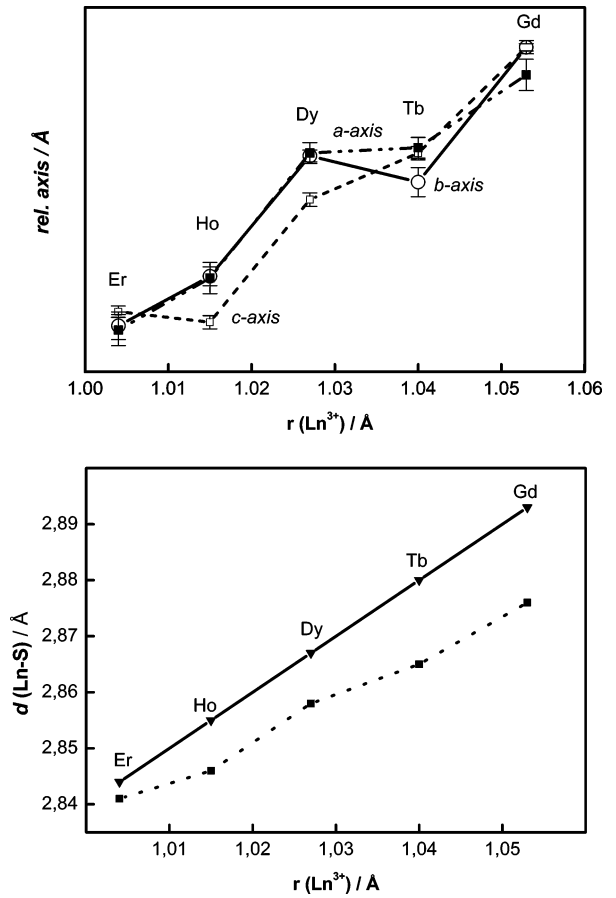

Figure 5. Evolution of the crystallographic axes across the series $Ba_3Ln_2[P_4S_{16}]$ (Ln = Er, Ho, Dy, Tb, Gd) (top) and of the Ln−S distances (bottom).

S−P(1)−S and S−P(2)−S angles are identical (109.4° for both).

A new and unusual feature of the structure of the isostructural title compounds compared to those of the hitherto known RE thiophosphates is the formation of helical chains. The occurrence of anionic helices is unique in the chemistry of RE compounds containing the $[PQ_4]^{3-}$ tetrahedron. The special connection modes between the LnS_8 polyhedra and the $[PS_4]^{3-}$ tetrahedra are responsible for the formation of these chains, and in the following, the differences between connection modes found in the title compounds and in other RE chalcogenophosphates are highlighted.

In the structures of RE chalcogenophosphates, the $[PQ_4]^{3-}$ anion connects a different number of Ln ions, and the connection schemes exhibit various motifs. In addition, LnQ_x polyhedra are joined in a different manner with each other (Figure 6a−g). Note that only those $[PQ_4]^{3-}$ groups are drawn that show the highest coordination to Ln atoms in each compound. From Figure 6a−g, it is obvious that one $[PQ_4]^{3-}$ tetrahedron can bridge two, three, four, and six Ln ions, and each compound can be classified by the number of neighboring RE atoms sharing S atoms with each other and the $[PQ_4]^{3-}$ unit. For example, in $TlEu[PS_4]$[14] (Figure 6b) and $KEu[PS_4]$[23,24] (Figure 6c), the central $[PS_4]^{3-}$ tetrahedron is joined to four EuS_6 prisms. But in $KEu[PS_4]$, two adjacent EuS_6 polyhedra share common edges, leading to the formation of a layered anion; in $TlEu[PS_4]$, the analogous EuS_6 prisms have no common S atom, and a three-dimensional anionic network is observed.

The closest relationship to the structure of the title compounds exists in $K_3La[P_2S_8]$[24] (**I**; Figure 6d) and $K_3Ce_2[P_3S_{12}]$[28] (**II**; Figure 6f). The anionic part of $Ba_3Ln_2[P_4S_{16}]$ may be derived from $K_3La[P_2S_8]$ by simply doubling the formula unit, leading to $La_2[P_4S_{16}]^{6-}$. Due to the presence of Ba^{2+} instead of K^+, a different structure type is observed. In both compounds, one-dimensional anionic chains are present, but the topology of the chains differs because of a different bonding of the $[PS_4]^{3-}$ units. As in $Ba_3Ln_2[P_4S_{16}]$, there are two distinct P atoms in **I**. But in **I**, the $[PS_4]^{3-}$ tetrahedron joins only two Ln^{3+} ions via two common edges, and each tetrahedron has one terminal S atom (Figure 6d). In contrast, the $[P(1)S_4]^{3-}$ unit in $Ba_3Ln_2[P_4S_{16}]$ bridges three Ln^{3+} centers via three common edges, whereas the $[P(2)S_4]^{3-}$ group has a common edge with only one LnS_8 prism, i.e., two S atoms are terminal. The different binding modes between the $[PS_4]^{3-}$ tetrahedra and the LnS_8 polyhedra in the two compounds lead to linear chains along [100] in **I** and the above-mentioned helical chains in $Ba_3Ln_2[P_4S_{16}]$.

The arrangement of the Ba(1) and K(2,1) ions are comparable, i.e., they separate the chains running parallel to [001] and [100], respectively. But the environments of the Ba(2) and K(3) ions are different (Figure 7). The Ba(2) atom is surrounded by six $[PS_4]^{3-}$ tetrahedra, and shares

(36) Shannon, R. D. *Acta Crystallogr., Sect. A* **1976**, *32*, 751.

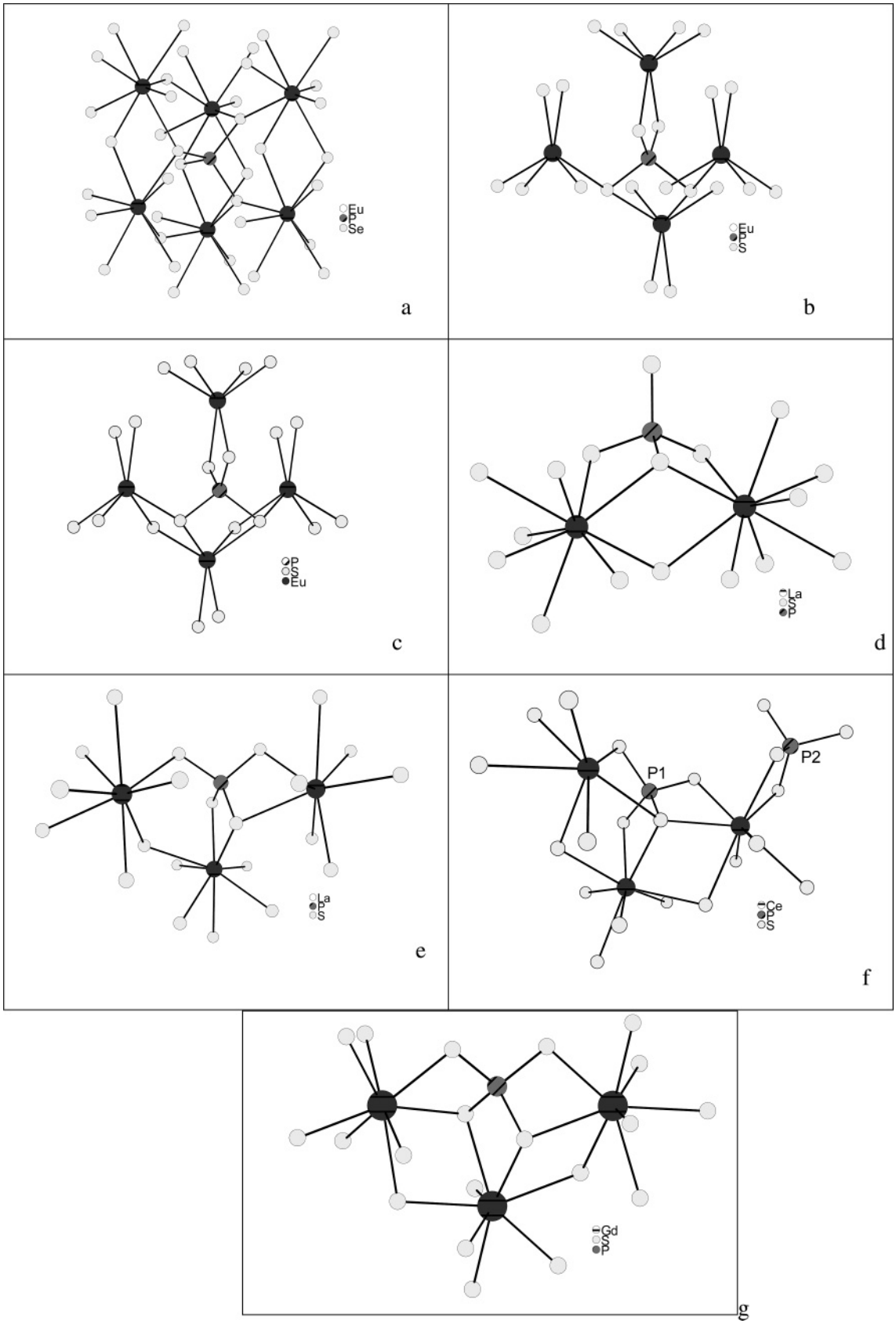

Figure 6. Connection mode of $[PS_4]^{3-}$ tetrahedra in RE thiophosphates. (a) $LiEu[PSe_4]$, (b) $TlEu[PS_4]$, (c) $KEu[PS_4]$, (d) $K_3La_2[P_2S_8]$, (e) $K_2La[P_2S_7]$, (f) $K_3Ce_2[P_3S_{12}]$, and (g) $Ba_3Gd_2[P_4S_{16}]$.

edges with two of them (Figure 8, right). The K(3) ion is bound to four $[PS_4]^{3-}$ units, and has common edges with all tetrahedra (Figure 8, left). Because of the smaller ionic radius of Ba^{2+} and the special arrangement of the anionic chains, the shortest interlayer distance is smaller in $Ba_3Ln_2[P_4S_{16}]$ than in $K_3La[P_2S_8]$.

As noted above, the structure of the title compounds also has a close relationship to that of $K_3Ce_2[P_3S_{12}]$ (**II**). The

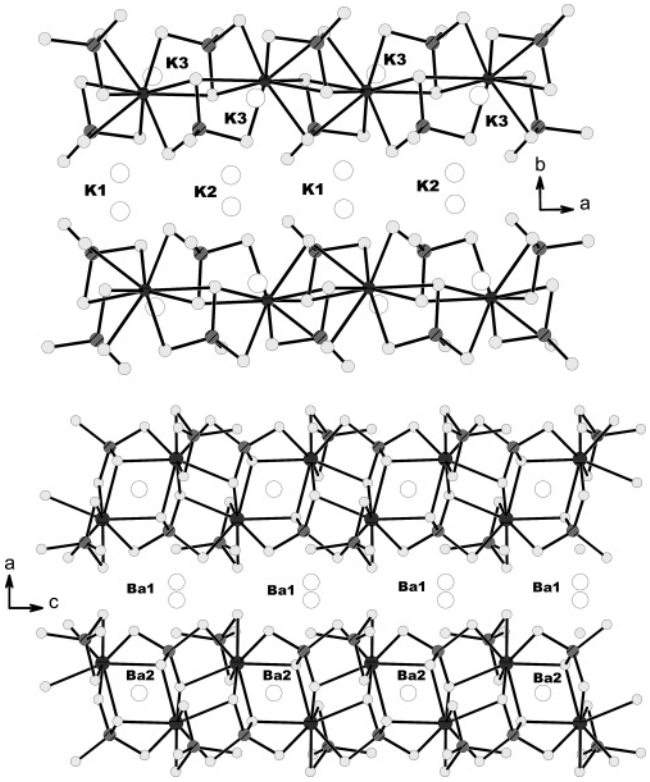

Figure 7. Different arrangement of the cations in compounds $K_3La[P_2S_8]$ (top) and $Ba_3Ln_2[P_4S_{16}]$ (bottom).

formal condensation of two anionic chains via a $[PS_4]^{3-}$ unit yields layered anions in **II**. One Ln ion of one chain shares two S atoms of the $[PS_4]^{3-}$ anion of the other chain, and the formation of the chains in the title compound may be formulated as $[Ln_2P_3S_{12}]^{3-} + [PS_4]^{3-} \rightarrow [Ln_2P_4S_{16}]$,$^{6-}$ which is schematically shown in Figure 9. When comparing the two structures, we should highlight another interesting feature. In both structures, the central $[PS_4]^{3-}$ tetrahedron connects three LnS_8 polyhedra via common edges. But in **II**, one S atom of the $[PS_4]$ group has bonds to all three Ln^{3+} ions, and the remaining S atoms are bound to only one Ln^{3+} ion; in the title compounds, two S atoms join two Ln^{3+} ions, and the other two S atoms have only one bond to one Ln^{3+} ion. In conclusion, the structure of $Ba_3Ln_2[P_4S_{16}]$ may be regarded as being a derivative of a hypothetical $A_6Ln_2[P_4S_{16}]$ (A = alkaline cation) compound.

Interestingly, the synthesis of $Ba_3Ln_2[P_4S_{16}]$ with the larger Ln^{3+} ions (La−Eu) was not successful. Under identical reaction conditions, Ln[PS_4] (Ln = La, Ce, Pr, Nd) as well as $Eu_2[P_2S_6]$ and $Ba_2[P_2S_6]$ were formed. The influence of the size of the Ln^{3+} ions on the structures is well documented, and examples are NaSm[P_2S_6] and NaYb[P_2S_6][25] or the KLn-[P_2Se_6] family.[17] Structural variations are found due to the larger Ln^{3+} ions' preference for higher coordination numbers. For $Ba_3Ln_2[P_4S_{16}]$, an insertion of La−Sm should not lead to a different structure type because Ln^{3+} ions are in an environment of 8 S atoms, which is often observed for La−Sm. The reason compounds with the larger Ln^{3+} ions are not crystallizing with the structure of the title compounds is not fully understood. It is well-known that the size and charge of counterions influence the dimensionality of crystal structures.[37] In the present case, the size of Ba^{2+} remains constant. But when larger Ln^{3+} ions are introduced, the anionic part $[Ln_2P_4S_{16}]^{6-}$ becomes bulkier due to the elongation of Ln−S bonds. From a formal point of view, the negative charges are distributed over a larger volume, making the anion softer. Within the framework of hard and soft acids and bases, the hard Ba^{2+} ion cannot stabilize the soft anion. If this is the reason, compounds with larger Ln^{3+} ions crystallizing in the structure of the title compound cannot be prepared because no softer alkaline-earth cation is available (except Ra^{2+}). One can also speculate that under the synthesis conditions, the ternary Ln[PS_4] compounds (Ln = La, Ce, Pr, Nd, Sm) are thermodynamically more stable than quaternary $Ba_3Ln_2[P_4S_{16}]$ compounds with Ln = La, Ce, Pr, Nd, and Sm. Syntheses of compounds with composition $A_3Ln_2[P_4S_{16}]$ (A = Ca, Sr) are underway by applying the Ln^{3+} ions with the smallest ionic radii, i.e., Ln = Tm, Yb, and Lu.

Vibrational Spectroscopy. MIR, far-IR, and Raman spectra were recorded for $Ba_3Ln_2[P_4S_{16}]$ (Ln = Gd, Er). Corresponding vibrational frequencies, intensities, and their assignments are given in Table 4.

The spectroscopically relevant unit is $[PS_4]^{3-}$. Free $[PS_4]^{3-}$ ions possess T_d symmetry with $\Gamma(T_d) = A_1 + E + 2F_2$.[38] All vibrations are Raman-active, whereas just the two F_2 races are IR-active. Both the crystallographic [PS_4] tetrahedra possess site symmetry C_1, and due to this symmetry, the point group analyses result in $\Gamma = 9A$. Therefore, all 3N-6 vibrations should be observed in the Raman as well as in the IR spectra. Absorptions in the region from 650 cm^{-1} to approximately 450 cm^{-1} are necessary for stimulating P−S vibrations, whereas for Ln−S and Ba−S vibrations, lower energies are required. Despite the fact that no data for [PS_4] tetrahedra with C_1 site symmetry are reported, the experi-

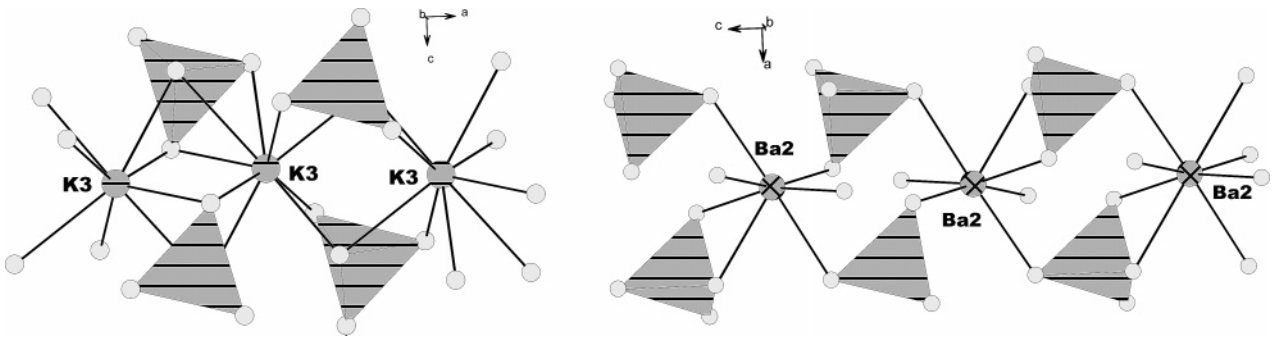

Figure 8. Environment of K(3) in $K_3La[P_2S_8]$ (left) and Ba(2) in $Ba_3Ln_2[P_4S_{16}]$ (right).

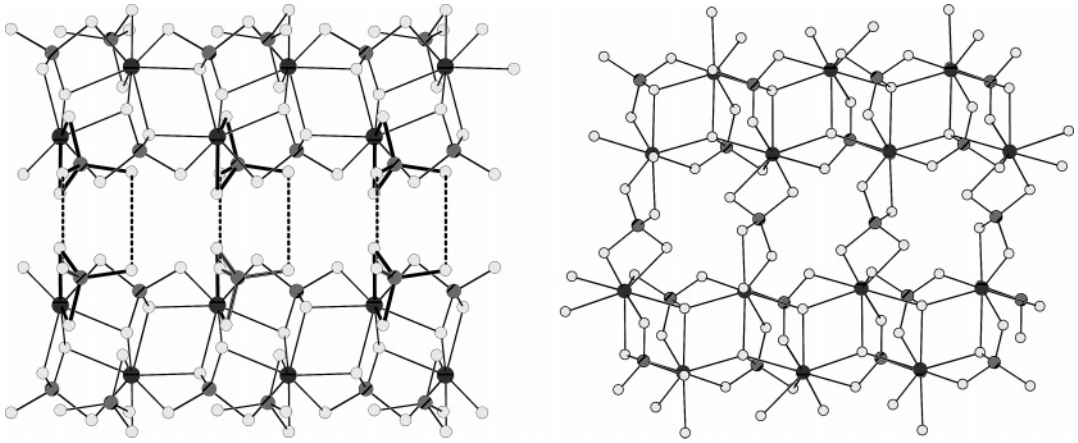

Figure 9. Schematic representation of the condensation of isolated chains in $Ba_3Ln_2[P_4S_{16}]$ (left) to layers via bridging $[PS_4]^{3-}$ units in $K_3Ce_2[P_3S_{12}]$ (right) (Ba^{2+} and K^+ ions are not displayed).

Table 4. Vibrational Frequencies (cm^{-1}) of $Ba_3Ln_2[P_4S_{16}]$ (Ln = Gd, Er), Intensities, and Proposed Assignment in Comparison to the Free $[PS_4]^{3-}$ Vibrations[a]

free $[PS_4]^{3-}$ [42]	IR/FIR (Er)	IR/FIR (Gd)	Raman (Er)	Raman (Gd)
		Stretching Vibrations		
	639 w	636 w	647	
	615 s	613 s	612 vw	610 vw
	596 s	594 s	596 vw	592 vvw
ν_3 (F_2): 548	585 s	582 s	574 vvw	573 vvw
	560	558	568 vw	563 vvw
	550	547	555 w	553 vvw
	528 vs	524 vs	528 w	525 vw
	448 m	**448**		
ν_1 (A_1): 416	433 m	429 m	435 m	431 vs
	414 vw	412 vw	415 m	414 s
			389 s	**389 s**
		Bending Vibrations		
			311 w−m	**311 w−m**
	299 s	298 s	298 m	299 w−m
	292 s sh	290 s	290 w−m	289 w−m
ν_4 (F_2): 270	**285 s**	**285 s**		
	277 m	277 m sh	282−272 w sh	282−272 w sh
	271 s	272 s	282−272 w sh	282−272 w sh
			264 w−m	**259 w−m**
	255 w−m	**255 w−m**		
	239 vw	240 vw	244	245
ν_2 (E_1): 215	214 vw	214 vvw	213	214

[a] s = strong, m = medium, w = weak, v = very, sh = shoulder. Absorptions that are not observed in both the Raman and IR spectra are rendered in bold.

mental data and the assignment of the P−S vibrations are comparable with data given in the literature,[39−41] and enable the tentative assignment of the ν_3 and ν_1 modes to the F_2 and A_1 race. The assignment of the ν_4 and ν_2 modes to the other F_2 and the E race[42] seems to be more uncertain, because these absorptions may already be due to Ln−S or Ba−S vibrations.

The EDX analysis gives hints of some impurities with $Ba_2[P_2S_6]$,[43] which could actually be assigned to those vibrations that are not observed in the far-IR and Raman spectra. For $Ba_2[P_2S_6]$, the spectroscopically relevant unit is the $[P_2S_6]^{4-}$ anion. The vibrations at 448, 285, and 255 cm^{-1} observed in the far-IR spectra are not found in the Raman spectra. The comparison with data given in ref 3 shows that the vibrations belong to non-Raman-active vibrations of $[P_2S_6]^{4-}$ in $Eu_2[P_2S_6]$, which is isostructural with $Ba_2[P_2S_6]$ (lit.: 446 cm^{-1}, m; 286 cm^{-1}, s; 255 cm^{-1}, m). The absorptions at 389 and ∼260 cm^{-1} are observed only in the Raman spectra, and can also be assigned to $[P_2S_6]^{4-}$ vibrations that are in this case only Raman-active (lit.: 389 cm^{-1}, vs; 261 cm^{-1}, w−m). However, no assignment can be given for the vibrations at 264 cm^{-1} (Er) and 259 cm^{-1} (Gd). The absorptions at 311 cm^{-1}, which are not IR-active, cannot be assigned to $[PS_4]^{3-}$ or $[P_2S_6]^{4-}$ vibrations, but nevertheless they may already be caused by Ln−S/Ba−S vibrations. Some absorptions at lower energies are tendentiously shifted to higher energies for Gd, whereas all the $[PS_4]^{3-}$-unit-assigned vibrations above 311 cm^{-1} are shifted to lower energies. For the excitation of Ln−S vibrations, higher energies for lighter Ln ions are expected; therefore, these peaks may be assigned to Ln−S vibrations (Raman: 179 cm^{-1} (Gd), 177 cm^{-1} (Er); FIR: 178 and 157 cm^{-1} (Gd), 174 and 153 cm^{-1} (Er)).

Optical Spectroscopy. For the determination of the optical band gaps, we performed reflection measurements at room temperature for all compounds. The respective spectrum of $Ba_3Gd_2[P_4S_{16}]$ is shown in Figure 10. In this case, no $4f^7 \rightarrow 4f^7$ transitions are detected in the visible range, because the first excited $4f^7$ state is at about 32 000 cm^{-1}.[44] The band gaps were estimated to be at approximately 3.41 eV (Gd) (27 500 cm^{-1}, 364 nm), 3.37 eV (Tb) (27 180 cm^{-1}, 368 nm), 3.28 eV (Dy) (26 450 cm^{-1}, 378 nm), and 3.3 eV (Ho, Er) (26 615 cm^{-1}, 376 nm). The values for Tb, Dy, Ho, and Er are only lower limits, because there might be some $4f^n \rightarrow 4f^n$ transitions that overlie the band transition (Figure 11). In any case, the band gaps correspond to an UV absorption;

(37) Kanatzidis, M. G. *Phosphorus, Sulfur Silicon Relat. Elem.* **1994**, *93−94*, 159.
(38) Weidlein, J.; Müller, U.; Dehnicke, K. *Schwingungsspektroskopie: eine Einführung;* K. G. Thieme Verlag: Stuttgart, Germany, 1982.
(39) Becker, R.; Brockner, W.; Eisenmann, B. *Z. Naturforsch.* **1987**, *42A*, 1309.
(40) Becker, R. Ph.D. Thesis, Technische Universität Clausthal, Clausthal-Zellerfeld, Germany, 1988.
(41) Derstroff, V.; Ensling, J.; Ksenofontov, V.; Gütlich, P.; Tremel, W. *Z. Anorg. Allg. Chem.* **2002**, *628*, 1346.
(42) Müller, A.; Mohan, N.; Christophliemk, P.; Tossidis, I.; Dräger, M. *Spectrochim. Acta, Part A* **1973**, *29*, 1345.
(43) Sörens, S.; Mewis, A.; Hoffmann, R.-D.; Pöttgen, R.; Mosel, B. D. *Z. Anorg. Allg. Chem.* **2003**, *629*, 429.
(44) Dieke, G. H. *Spectra and Energy Levels of Rare Earth Ions in Crystals*; Interscience Publishers: New York, 1968.

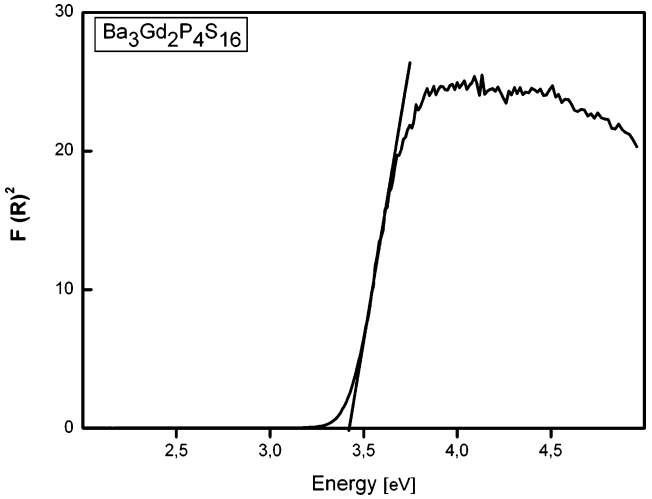

Figure 10. Reflectance spectrum of $Ba_3Gd_2[P_4S_{16}]$.

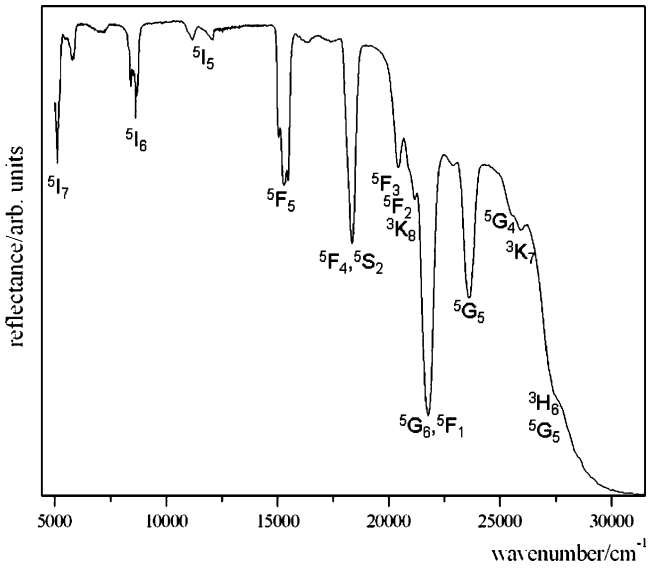

Figure 11. Reflectance spectrum of $Ba_3Ho_2[P_4S_{16}]$.

therefore, it is possible to investigate the $4f^n \leftrightarrow 4f^n$ transitions in the visible and NIR range.

For the investigation of 4f ↔ 4f transitions, we carried out reflectance as well as luminescence investigations on $Ba_3Ho_2[P_4S_{16}]$. In this case, the optical properties of $Ba_3Ho_2[P_4S_{16}]$ are of some interest because of the relatively strong luminescence compared to other Ho compounds, although the 17-fold degeneration of the ground state ($^5I_8$) as well as those of the excited states makes luminescence studies rather difficult.[45]

The reflectance spectrum of $Ba_3Ho_2[P_4S_{16}]$ is depicted in Figure 11. Most of the peaks can be assigned to transitions from the $^5I_8$ ground state to $4f^{10}$ excited states of Ho^{3+} (Table 5). There are, however, some rather small peaks that cannot be assigned. The assignment of $4f^n \rightarrow 4f^n$ transitions to other rare earth ions that might be present as impurities is not very plausible. The most frequent lanthanide impurities for Ho^{3+} should be the neighboring ions (i.e., Tb, Dy, Er, Tm), but the peaks in the present spectrum cannot be assigned to these ions.[44] Also, absorption starting from excited states cannot be responsible, because the first excited state is located at >5000 cm^{-1}; therefore, it is not occupied at room temperature. The spectrum shown in Figure 11 depicts some strong absorption in the visible as well as in the NIR range. The strongest ones are transitions from the $^5I_8$ ground state to the $^5F_5$ state at 15 291 cm^{-1} as well as to $^5F_4$, $^5S_2$ at 18 349 cm^{-1}, and to $^5F_1$, $^5G_6$ states at 21 786 cm^{-1}. This intensity distribution is typical for Ho^{3+} ions, and is comparable to that of, for example, Ho^{3+} ions in aqueous solution,[46] although the intensity ratio $^5I_8$:$^5G_6$/$^5I_8$:$^5F_4$, $^5S_2$ is larger in the present case. This circumstance is responsible for the yellow color of the compound. Due to the manifold of the crystal-field levels of both ground and excited states with a maximum value caused by the C_1 symmetry of the Ho site, they are not resolved because of the relatively low resolution of the measurement (1 nm).

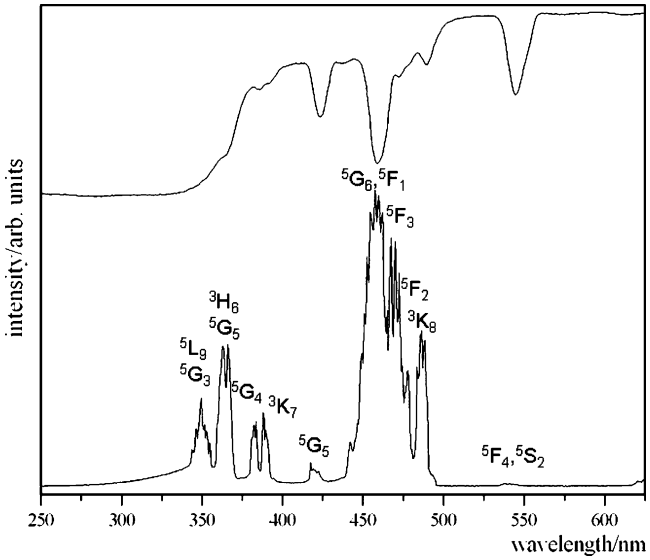

Figure 12. Reflectance spectrum (upper trace, RT) and excitation spectrum (lower trace, 77 K) of $Ba_3Ho_2[P_4S_{16}]$. The excited $4f^{10}$ levels are indicated. λ_{em} = 664.5 nm ($^5F_5 \rightarrow {}^5I_8$).

Table 5. Energy of the $^5I_8 \rightarrow 4f^{10}$ Transitions of $Ba_3Ho_2[P_4S_{16}]$ Observed in the Reflectance Spectrum

energy (nm) (energy (cm^{-1}))	excited state
1949 (5131)	$^5I_7$
1160 (8621)	$^5I_6$
896 (11 161)	$^5I_5$
654 (15 291)	$^5F_5$
545 (18 349)	$^5F_4$, $^5S_2$
490 (20 408)	$^5F_3$
477 (20 964)	$^5F_2$
472 (21 186)	$^3K_8$
459 (21 786)	$^5G_6$, $^5F_1$
424 (23 585)	$^5G_5$
392 (25 510)	$^5G_4$
386 (25 907)	$^3K_7$

The respective excitation spectrum shows some remarkable differences. In Figure 12, the excitation spectrum measured at 77 K in the range 250−650 nm with an emission detection at λ_{em} = 664.5 nm ($^5F_5 \rightarrow {}^5I_8$ transition) is depicted. For comparison, the reflectance spectrum in this range is also included in the figure. The resolution of the excitation

(45) Görller-Walrand, C.; Binnemans, K. *Handbook on the Physics and Chemistry of Rare Earths*; Gschneidner, K. A., Jr., Eyring, L., Eds.; Elsevier: Amsterdam, 1996; Vol. 23, Chapter 155, p 121.

(46) Binnemans, K.; Görller-Walrand, C. *Chem. Phys. Lett.* **1995**, *235*, 163.

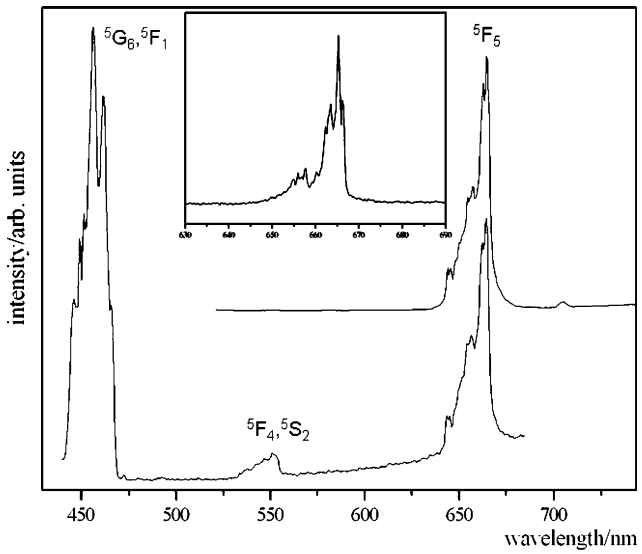

Figure 13. Emission spectra of $Ba_3Ho_2[P_4S_{16}]$ at 77 K. The excited $4f^{10}$ levels are indicated. Upper trace: $\lambda_{ex} = 478$ nm ($^5I_8 \rightarrow {}^5F_2$); lower trace: $\lambda_{ex} = 366$ nm ($^5I_8 \rightarrow {}^3H_6$). The high-resolution $^5F_5 \rightarrow {}^5I_8$ transition is shown in the inset.

spectrum is much higher because of cooling and the higher resolution (0.5 nm) during this measurement; however, it is also not possible to resolve the crystal-field levels in this case. Again, the $^5G_6$, $^5F_1$ transition has the largest intensity, but the intensities of other excitation bands differ notably from those of the reflectance spectrum. Whereas the $^5I_8 \rightarrow {}^3K_8$, $^5I_8 \rightarrow {}^5F_2$, and $^5I_8 \rightarrow {}^5F_3$ transitions show higher intensities in the excitation spectrum, the intensities of transitions to $^5F_4$, $^5S_2$, and $^5G_5$ excited states are much lower compared to those of the reflectance spectrum. Obviously, excitation to the latter leads to relaxation pathways other than the $^5F_5 \rightarrow {}^5I_8$ emission (see below). In the excitation spectrum, no transitions above 340 nm (29 410 cm^{-1}), i.e., in the conduction band of $Ba_3Ho_2[P_4S_{16}]$, could be detected, although some excited $4f^{10}$ states are present in this range.[44] Apparently, excitation to these states leads to relaxation in a way that is different from $^5F_5 \rightarrow {}^5I_8$ emission.

The low-temperature emission spectrum of $Ba_3Ho_2[P_4S_{16}]$ excited at $\lambda_{ex} = 366$ nm ($^5I_8 \rightarrow {}^3H_6$) shows two large emission bands (Figure 13, lower trace), which causes a reddish-blue emission of the compound. Such a strong emission is rather unusual for Ho^{3+} compounds.[47] The observed bands can be assigned to the $^5F_5 \rightarrow {}^5I_8$ ($\lambda_{max} = 664.5$ nm, 15 050 cm^{-1}) and $^5G_6$, $^5F_1 \rightarrow {}^5I_8$ ($\lambda_{max} = 456.5$ nm, 21 906 cm^{-1}) transitions, although the latter has more than twice the intensity of the former. Besides the strong $^3H_6 \rightarrow {}^5I_8$ emission, $^5I_8 \rightarrow {}^5F_2$ excitation also yields weak $^5F_4$, $^5S_2 \rightarrow {}^5I_8$ ($\lambda_{max} = 551$ nm, 18 150 cm^{-1}) emission bands, which are not detectable in the case of low energetic excitation at 478 nm (Figure 13, upper trace). In the emission spectrum, the crystal-field levels are also not resolved. This is clearly shown for the $^5F_5 \rightarrow {}^5I_8$ transition; the high-resolution (0.2 nm) spectrum is presented as an inset in Figure 13. Because of the large number of crystal-field levels in both states, 187 single transitions are expected at maximum. This number is clearly not observed, although some transitions are expected to be too low in intensity to be detected.

In general, an interpretation of the luminescence spectra of Ho^{3+} ions is rather complicated because of the crowded energy-level diagram. This is also true in the present case. The strong luminescence observed for $Ba_3Ho_2[P_4S_{16}]$ is quite strange, as multiphonon relaxation should occur because the highest phonon energy is present at more than 600 cm^{-1}. This is especially the case for the strong $^5G_6$, $^5F_1 \rightarrow {}^5I_8$ emission, because the $^5F_3$, $^5F_2$, and $^3K_8$ states are located at a slightly lower energy (Figures 12 and 13). The different intensities of the transitions in the luminescence spectra compared to those of the reflectance spectra can be explained in some cases, however, by cross relaxation. As an example, the low intensity of the $^5F_5 \rightarrow {}^5I_8$ emission after $^5I_8 \rightarrow {}^5F_4$, $^5S_2$ excitation is explained by cross relaxation between ($^5F_4$, $^5S_2 \rightarrow {}^5I_4$) and ($^5I_8 \rightarrow {}^5I_7$) states. Although the $^5I_4$ states are not observed in the reflectance spectrum, their position is expected to be at about 13 000 cm^{-1},[44] slightly more than 5000 cm^{-1} below the $^5F_4$, $^5S_2$ states and about 2300 cm^{-1} below the $^5F_5$ states, so that no $^5F_5 \rightarrow {}^5I_8$ emission can be detected after cross relaxation. This phenomenon is in fact observed in the case of $LaCl_3$:Ho^{3+}.[48] For $LaCl_3$, the La−La distances are 4.37 and 4.84 Å,[49] and are thus very comparable to Ho−Ho distances in $Ba_3Ho_2[P_4S_{16}]$ (4.43 and 4.77 Å, Table 3). Also, cross relaxation between ($^5G_5 \rightarrow {}^5F_4$, $^5S_2$) and ($^5I_8 \rightarrow {}^5I_7$) may occur, because the energies of both transitions fit well. This may be followed by the above-mentioned cross relaxation, which would explain the low intensity of the $^5I_8 \rightarrow {}^5G_5$ transition in the excitation spectrum. There may also be some other cross relaxation pathways that lead to the present observations. A more detailed spectroscopic investigation is, however, necessary for proof.

Conclusion

The successful synthesis of the first alkaline-earth rare earth thiophosphates is a first step for a new and exciting chemistry of materials that may have unexpected structural and physical properties. It can be assumed that many more compounds could be made available by varying the synthesis conditions. Obviously, the structure family with composition $(A_4P_2Q_6)_l(A_3PQ_4)_m(Ln_4(P_2Q_6)_3)_n(LnPQ_4)_o$ ($l = 0$, $m = 2$, $n = 0$, $o = 2$) offers a large variation of different parameters, i.e., stoichiometry and/or the type of the A cations. The structure of the title compounds with the helical $[Ln_2(PS_4)_4]_n^{6n-}$ chains is unique in rare earth chemistry, and demonstrates the high level of flexibility of both the coordination behavior of Ln^{3+} ions and the binding modes of $[PS_4]^{3-}$ anions. Not only are the compounds interesting from a structural point of view but they also exhibit highly interesting optical properties. Because of the presence of alkaline earth ions, doping with Eu^{2+} ions should be possible. This would lead to compounds containing both di- and trivalent rare earth ions, and exceptional behavior (e.g., energy transfer between the lanthanoid ions) can be expected in this case.

Acknowledgment. We thank I. Jess for the single-crystal work. Financial support by the State of Schleswig-Holstein and

(47) Shionoya, S.; Yen, W. M. *Phosphor Handbook*; CRC Press: Boca Raton, FL, 1999.
(48) Porter, J. F., Jr. *Phys. Rev.* **1966**, *152*, 300.
(49) Morosin, B. *J. Chem. Phys.* **1968**, *49*, 3007.

the Deutsche Forschungsgemeinschaft (DFG, SPP 1166) is gratefully acknowledged.

Supporting Information Available: Tables of crystal data, structure solution and refinement, atomic coordinates, bond lengths and angles, and anisotropic thermal parameters for the compounds (cif files in pdf format). This material is available free of charge via the Internet at http://pubs.acs.org.

CM051860N